Magnetite layer formation in the Bushveld Complex of South Africa

Zhuo-Sen Yao
Carleton University
James Mungall (jamesmungall@cunet.carleton.ca)
Carleton University https://orcid.org/0000-0001-9726-8545

Article

Keywords: magnetite layer formation, South Africa, Bushveld Complex

Posted Date: July 13th, 2021

DOI: https://doi.org/10.21203/rs.3.rs-673073/v1

Version of Record: A version of this preprint was published at Nature Communications on January 20th, 2022. See the published version at https://doi.org/10.1038/s41467-022-28000-9.

Magnetite layer formation in the Bushveld Complex of South Africa

Zhuo-sen Yao and James E. Mungall*

Department of Earth Sciences, Carleton University, Ottawa, Ontario K1S 5B6, Canada

Abstract

The great economic significance of layered mafic-ultramafic intrusions like the Bushveld Complex of South Africa results from the existence within them of some layers highly concentrated in valuable elements. Here we address the origins of the Main Magnetite Layer, a globally important resource of Fe-Ti-V-rich magnetite. Previous models of *in situ* fractional magnetite crystallization require frequent *ad hoc* adjustments to the boundary conditions. An alternative model of rapid deposition of loose piles of magnetite crystals followed by compositional convection near the top of the pile and infiltration of the pile from beneath by migrating intercumulus melt fits observations without any adjustments. The data admit both explanations, but the latter model, with the fewest unconstrained interventions, is preferable. The choice of models has pivotal ramifications for understanding of the fundamental processes by which crystals accumulate and layers form in layered intrusions.

Introduction

Because it is impossible to observe directly the processes that produce layered plutonic mafic rocks, the nature of these processes must be inferred from the record of composition, mineral mode, and texture of the final products of emplacement, crystallization, and cooling of the magma[1]. Even the most basic of questions, such as whether or not crystals form within the melt and settle to the floor[2-3] or are nucleated and grow *in situ* (i.e., by heterogeneous nucleation in direct physical contact with the solid base)[4-5], remain open to controversy after a century of dedicated research effort. Progress will be difficult without resolution of such

fundamental questions. A common approach to attempt to resolve these matters is to produce a forward geochemical or physical model and use it to demonstrate the feasibility of a particular hypothetical process; however, there are many examples of cases where totally contradictory hypotheses can be framed in forward models that successfully match observations[6-7]. The resolution of these questions is of more than purely academic interest because some of the layers in question contain mineral deposits of global economic significance[8]. It is therefore essential to address the larger framework within which individual hypotheses are framed before we can make reasoned judgements about which ones to favor.

One deposit that has long been used as a laboratory to address the controls on layer formation in layered intrusions is the Main Magnetite Layer (MML) in the Upper Zone of the Rustenburg Layered Suite of the Bushveld Complex of South Africa[9-19]. Here we compare observations of the MML with some forward thermodynamic and fluid dynamic models, appealing to various combinations of fractional crystallization, compositional convection during adcumulus crystal growth, and reactive transport of upward-migrating Cr-rich melt from beneath the MML. By comparison of our models with previously published work we show that multiple model approaches can achieve similar results, with the result that no model can be used definitively to exclude any other; however, some models are intrinsically more appealing than others because they require fewer arbitrary adjustments to achieve a successful fit to the data. In the immediate context of mechanisms of layer formation in layered intrusions, we show that purportedly incontrovertible evidence for *in situ* crystallization of magnetite can better be used to support a role for melt infiltration from below an initially homogeneous magnetite crystal mush, but the choice of model remains a matter of preference.

The Upper Zone of the Bushveld Complex crystallized from an iron-rich basaltic andesite magma at the top of the Rustenburg Layered Suite in what appears to have been a melt-dominated sill hundreds of km wide and at least several hundred m deep[17]. The evolution of this magma and its cumulates can be modeled broadly as the product of a protracted process of fractional crystallization at the scale of the entire Upper Zone[3,17,20], however the Upper Zone contains at least 26 magnetitite layers that are ~0.1-10 m thick and concordant with the igneous layering. The formation of these magnetite layers cannot be accommodated by a simple process of fractional crystallization from a single homogeneous body of liquid the size of the entire Upper Zone. Instead, it seems probable that a repeated cyclic process of spontaneous double diffusive convection occurred wherein the rejected liquid complementary to the gabbroic cumulates was denser than the main body of magma, causing the system to become stratified with a dense Fe-rich residual melt separating the growing cumulate pile from the rest of the magma[17,21]. It is thought that when magnetite became saturated and a layer of magnetitite was crystallized from this dense Fe-rich layer the liquid density rapidly diminished, causing convective overturn and re-homogenization of the magnetite-depleted basal layer with the rest of the magma and terminating magnetite crystallization until the closing stage of the next such cycle. Magnetitite layers generally have sharp and smooth or undulating boundaries with underlying anorthosites, but grade upwards into magnetite-rich gabbro due to smoothly increasing plagioclase modal abundance[13,17]. Along with abundant anorthosite xenoliths, narrow plagioclase-rich layers are widely developed within magnetitite layers (Fig. 1). The other portions are composed almost entirely of magnetite with minor interstitial plagioclase and pyroxene, effectively constituting monomineralic adcumulates. The economically important Main Magnetite Layer (MML), near the bottom of the Upper Zone, has ~1-2.5 m thickness and crops out intermittently over hundreds of km of strike extent[10-14,22]. It has been the focus of efforts to explain magnetitite formation.

Although the origin of magnetitite layers has spurred an ongoing debate between various hypotheses[22], there has been general agreement that the magnetitite we observe now is an adcumulate evolved from a magnetite-dominated mush with a high initial amount of interstitial melt[13,23]. However, Kruger and Latypov[18] recently proposed that this mushy zone had negligible thickness, being deposited directly onto a solid substrate *in situ* to form magnetite adcumulates with little or no initial interstitial melt. The highly compatible behavior of Cr in magnetite[24] makes it sensitive to magmatic processes (e.g., crystallization and reactive melt infiltration), and the quasi-exponential vertically decreasing Cr gradients in monomineralic magnetitite layers have been widely attributed to fractional crystallization at or near the magma chamber floor[10-12,14-15,18]. Failure of a simple one-stage Rayleigh fractionation model to match observed compositional profiles (e.g., Fig. 1a-d) led to propositions that the supply of Cr was modulated by double-diffusive convection in overlying melt domains[10-12,14-15]. By repeatedly changing the Cr concentration in the melt, model trends could be produced that matched the data. Models of this sort can be shown to be consistent with observations but are not persuasive means to compare hypotheses when the boundary conditions are endlessly changeable, thus ensuring that a fit to the data can always be achieved.

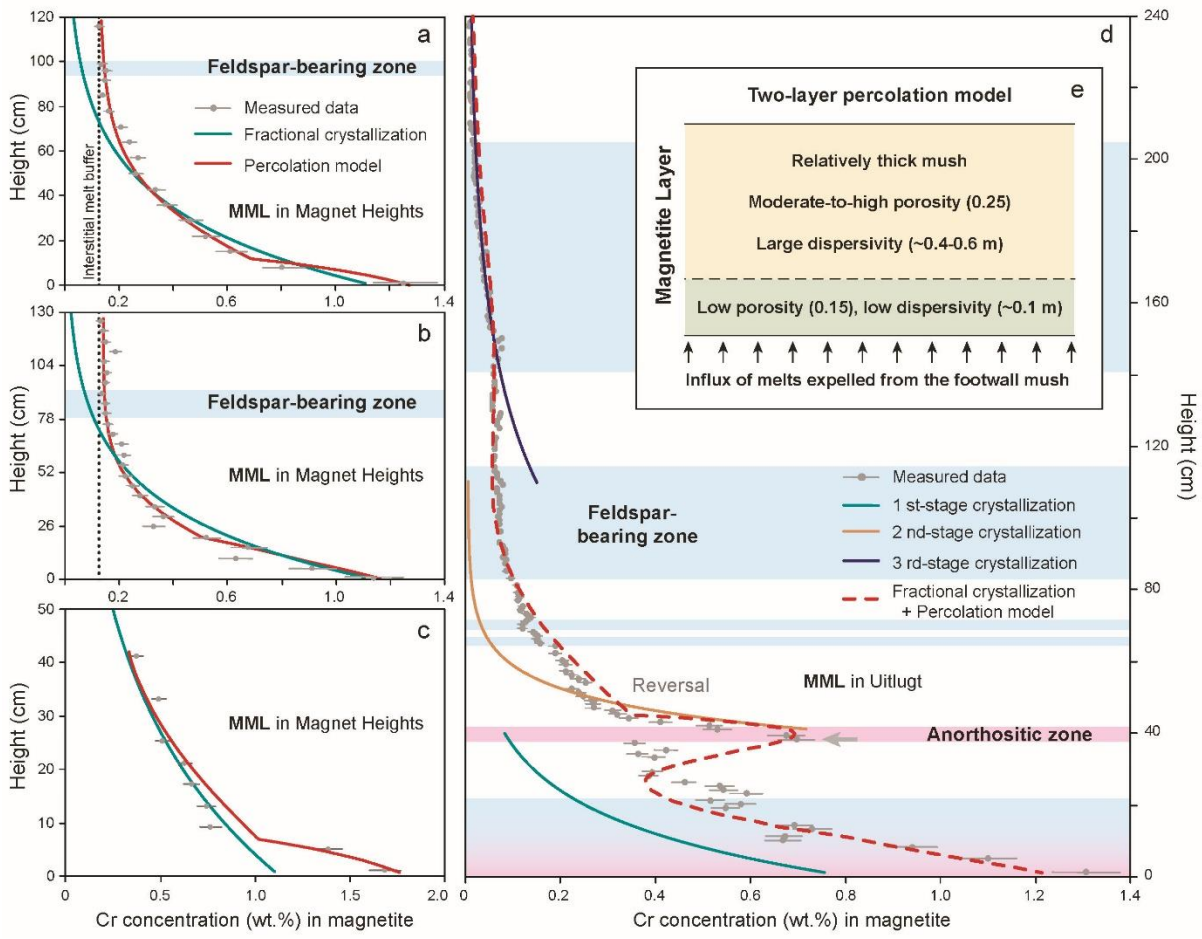

Fig. 1 (**a**-**d**) Measured and modeled vertical profiles of Cr contents in magnetite from the MML. Grey arrow in (**d**) reflects a major reversal in Cr content where a new crystallizing sequence began. (**e**) Diagram for the two-layer percolation model. All data collected from multiple sources cited in the text, e.g., profiles in (**a**-**b**)[22], (**c**)[18] and (**d**)[12].

Results

***Fractional crystallization models*.** Vertical profiles of Cr distribution in the MML, shown from Magnet Heights and Uitlugt in Figure 1, commonly show a curvilinear upward depletion from the bottom, which broadly matches expectations based on the compatibility of Cr during fractional crystallization of magnetite[10-12], but in each case the predictions do not match the data exactly. The Cr content decreases markedly more steeply at the base of every section, it locally shows extreme reversals (Fig. 1d), and it becomes constant at higher levels,

none of which it could do during fractional crystallization unless the melt composition or basic physical parameters changed repeatedly during the process[14-15]. A further complicating matter is the common occurrence of exceptionally Cr-rich nodes decorating the basal contact of the MML, showing strong lateral as well as vertical compositional gradients[16,18-19]. These features have been taken as evidence that magnetite initially nucleated and crystallized around discrete nodes which coalesced as they grew outwards and upwards[16,18].

We begin by addressing the profiles at Magnet Heights, shown in Figure 1a-c. The more complex Uitlugt profile will be addressed afterward. Here we assume that the MML is crystallized from a thick magma sheet, and that magnetite is the sole crystalline phase during the formation of the crystal mush of the MML (Methods). In Figure 1 we show models of fractional crystallization of magnetite from a homogeneous body of melt containing 57 ppm Cr[3,25], with f_{O2} between zero and one log unit below the quartz-fayalite-magnetite oxygen buffer (i.e., $-1 < \Delta QFM < 0$)[20,26-27] using a magnetite-melt partition coefficient of 200 at 1150 °C[14,24]. If the initial thickness of the overlying magma is set to 120 m as shown (Table 1), on the order of the vertical distance to the next magnetite layer up section[17,20,28], then the exponential decrease in Cr between 10 and 40 cm is reproduced by the model but in the upper portions of all of the profiles the model predicts much greater depletion of Cr than is observed. Furthermore, there is a short interval at the base of the MML in which Cr decreases much faster than predicted by the model (Fig. 1a-c). A simple model of fractional crystallization alone therefore only matches a short interval of the observed profile and is inadequate. Like our predecessors[14-15], we conclude that more complex processes have been at play.

131 We propose two mechanisms to account for the departures of the Magnet Hill Cr profiles
132 from fractional crystallization, both contingent on the assumption that the magnetitite
133 cumulate was initially solidified as a mush that retained some porosity occupied by interstitial
134 melt[13,23]. This could be consistent either with *in situ* crystallization or settling of magnetite
135 crystals formed by homogeneous nucleation. First, convection of intercumulus melt at the top
136 of the pile[29-30] might have promoted thorough re-equilibration of magnetite grains with the
137 overlying melt body (i.e., *compositional convection*) to homogenize the upper portions of the
138 pile and generate the flat profiles above ~60-80 cm in all profiles. Second, expulsion of Cr-
139 rich intercumulus melt from underlying anorthositic cumulates (i.e., *reactive melt infiltration*)
140 might have allowed upgrading of Cr contents in the basal parts of the layer. Both processes
141 depend on the rapid re-equilibration of magnetite crystals with percolating melt, which we
142 address below after considering the effects of compaction of the mush.
143
144 ***Compaction of magnetite mush.*** Isolated plagioclase crystals surrounded by magnetite
145 record weaker deformation than clustered grains, suggesting that magnetite mush contained
146 enough interstitial melt during early compaction to let the isolated crystals move or rotate
147 freely[23]. Poikilitic pyroxene in magnetitite commonly encloses many separate and loosely
148 packed subhedral-euhedral magnetite grains[13]; therefore, whether magnetite crystallized in-
149 situ or settled into place, there was initially substantial intercumulus melt. The sizes of the
150 primary grains (~0.5-2 mm) are similar with that of disseminated magnetite in associated
151 cumulate rocks, but far less than the crystals in silicate-free regions (~5-20 mm)[13], indicating
152 extensive overgrowth, compaction, and annealing to form the adcumulates. If it formed by a
153 process of fractional crystallization as a loose pile of settled crystals[3-4] or as a loose
154 arrangement of chains of magnetite crystals nucleated against others *in situ*[16,18-19] and
155 accumulated faster than the rate of compaction, the initial magnetite cumulate may have had

a high porosity (~0.52)[31]. Compaction is driven by the large density contrast between solid (~4955 kg·m^{-3}) and liquid (~2683 kg·m^{-3}) (Methods). Generally, this process initiates with a mechanical reorganization to achieve optimum packing and continues with pressure solution/reprecipitation and possible viscous deformation of cumulate minerals[29,31-33]. The thickness of the MML (<~2.4 m) may not have provided sufficient gravitational load and effective stress to drive plastic deformation of magnetite[23], and hence we argue that the compaction process was likely to have been achieved mainly through pressure solution and reprecipitation. On the basis of centrifuge experiments, Manoochehri and Schmidt[31] quantified the compaction rate for a chromite cumulate in basaltic magma via dissolution-precipitation compaction. Given the affinity between chromite and magnetite, here we assume that the rate of chemical compaction for a magnetite mush layer is similar to that for chromite cumulate. The required time to reduce porosity from the initial value (~0.52, the average porosity after crystal settling) to about 0.25 in a magnetite cumulate is in the range from 10 to 40 years, or even less if crystals are smaller (Fig. 2a; see Methods for details of this calculation).

Compositional convection and re-equilibration. While compaction is under way, continued crystallization of magnetite from intercumulus melt locally decreases the density of interstitial melt to a value lower than that of overlying magma, possibly causing it to rise as buoyant plumes into the overlying melt that must be convectively replaced by melt from the main magma body above the cumulate in the process of compositional convection[29-30].

During this process, the interstitial melt is continuously expelled and replaced by the overlying melt from the main magma body, maintaining a near-constant composition for the pore melt[29,34]. The occurrence of significant compositional convection requires that the

dimensionless local solutal Rayleigh number (R_a) exceeds a critical value of about 25[30,35] and that the characteristic convective velocity is higher than the rate of crystal accumulation[29]. The latter requirement is easily achieved in deep and large intrusions (e.g., the Upper Zone of the Bushveld Complex) due to the small accumulation rate (~0.1-1 m·year^{-1})[29]. Therefore, the minimum thickness of the magnetite cumulate pile to allow compositional convection to be operative can be estimated when the R_a value of porous medium equals the critical value (Methods). Figure 2b shows the minimum mush layer thickness to achieve the critical Rayleigh number permitting the onset of compositional convection for a range of grain sizes if the decrease of melt density is driven by the crystallization of a further 2.5 wt.% magnetite from the intercumulus melt. For example, convection begins when the thickness of an initial 1 mm-grained crystal mush exceeds ~0.44 m at 25% porosity (black dot in Fig. 2b), while a lower porosity (15%) will require a much thicker magnetite cumulate (~ 2 m, grey dot in Fig. 2b) for compositional convection. Compositional convection is therefore expected to operate in the loosely packed upper portion of the mush layer but will cease once compaction has reduced porosity.

During compositional convection and percolation, the interstitial melt will continuously modify the compositions of packed magnetite grains. Previous investigations have identified occurrences of compositionally heterogenous magnetite grains, but the observed systematic zonations of Al and Mg are solely related to the exsolution of spinel phases in the sub-solidus stage[36]. Some fluctuations of Cr occur in the rims of magnetite grains in contact with ilmenite or plagioclase and are also attributed only to the local sub-solidus re-equilibrium[36]. Observed lack of other types of zonation therefore indicates that any compositional modifications of magnetite grains driven by the convection and percolation are likely to have been completed in the early stage of post-cumulate processes. Re-equilibration between convecting interstitial

206 melt and magnetite grains involves two kinetic processes: the volume diffusion in single
207 magnetite grains and the diffusion of elements through a viscous and diffusive boundary
208 layer between the surrounding melt and magnetite (i.e., convective diffusion)[37]. The volume
209 diffusion of Cr in a magnetite grain is simplified as the penetration diffusion of Cr into a
210 spherical magnetite from an infinite source (i.e., interstitial melt)[38-39] (Methods). Due to the
211 relative motion between flowing interstitial melt and magnetite, the supply of nutrient for
212 magnetite growth is maintained fast enough to support our assumption of a constant boundary
213 composition on the surfaces of magnetite crystals for the volume diffusion[40]. Our models for
214 magnetite growth controlled by diffusion through a narrow boundary layer against a
215 convecting melt[40] and volume diffusion within solid magnetite[38-39] confirm that Cr-poor
216 grains (size < 1 cm) rapidly approach equilibrium with passing melt, and the required time is
217 reduced with increasing initial Cr contents of the grains (Fig. 2c-d). Most magnetite grains
218 would attain local equilibrium with the percolating melt in the post-cumulus stage, except for
219 the retention of Cr gradients in rare coarse crystals (> 1 cm)[36,41]. We therefore assume that Cr
220 content of magnetite in the dominant fine-grained population will be equilibrated with
221 percolating melts.
222
223 Based on the Cr content of clinopyroxene in the closest hanging wall of the MML[27], the
224 overlying magma is proposed to have contained ~6.2 ppm Cr after the formation of the
225 magnetite mush. Continuous loss of buoyant interstitial melt and its replacement by Cr-
226 depleted melt containing ~6.2 ppm Cr would maintain the upper magnetite grains at a
227 constant Cr content (~1240 ppm), which fits the profiles in Fig. 1a-b. Plagioclase can appear
228 in the sequence without any correlation to the Cr trend (Fig. 1), because in this situation Cr
229 content of magnetite has become decoupled from its initial value, whereas plagioclase would
230 resist diffusive re-equilibration because solid state diffusion is so slow in feldspar[42]. We

conclude that flattening of the profiles could have resulted from compositional convection within the magnetite mush rather than requiring changes in the composition or depth of the magma column from which it initially crystallized (cf. McCarthy and Cawthorn[12]).

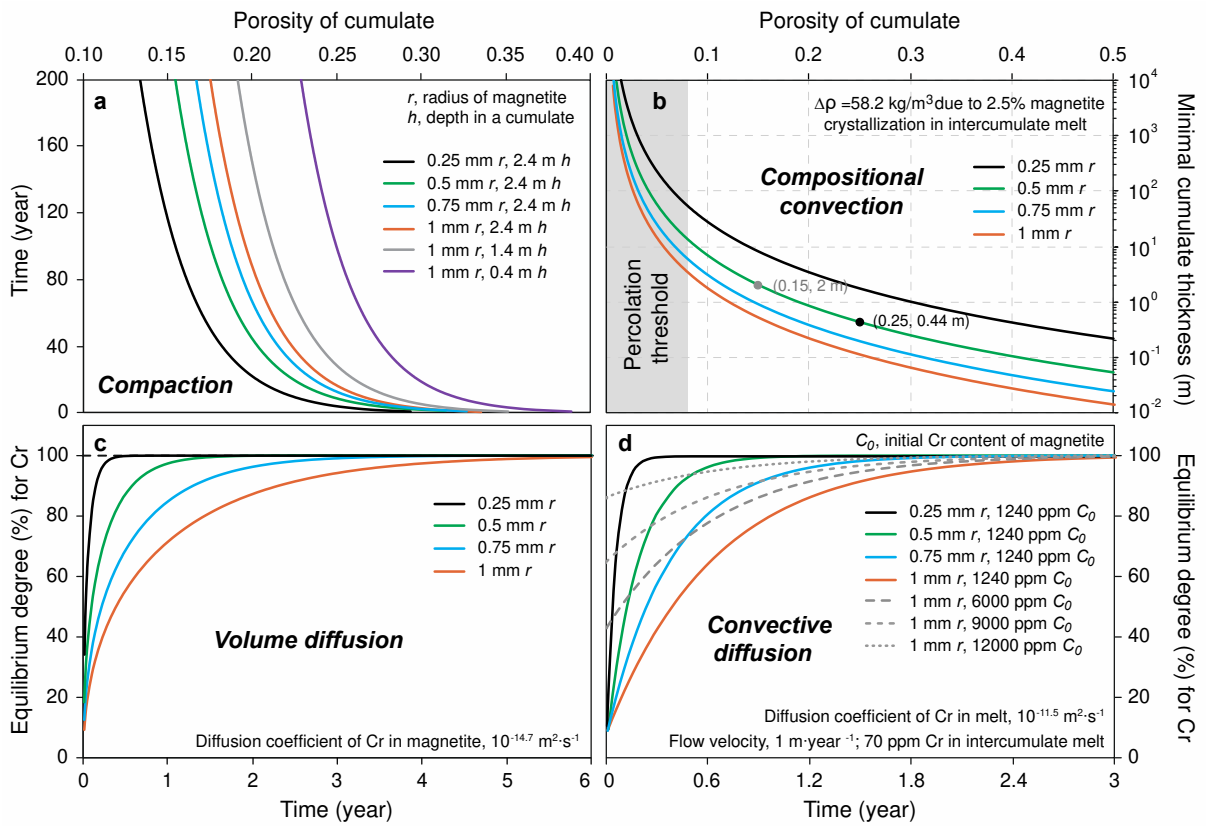

Fig. 2 Modeling results for (**a**) variation of magnetite mush porosity with time due to compaction; (**b**) Minimum thickness allowing compositional convection for mushes with indicated porosities. More thoroughly compacted lower portions of the mush may not spontaneously initiate compositional convection whereas more open upper portions could; (**c**) Approach of the bulk composition of magnetite grains (integrated over the entire diffusion profile) during volume diffusion of Cr due to re-equilibration of magnetite with migrating intercumulus melt; (**d**) Approach of bulk composition to equilibrium via convective diffusion for various sizes and initial Cr contents of magnetite. Coloured lines are for crystal sizes as in (**a, c**), and dashed lines represent magnetite grains with different initial Cr contents. Time scales of diffusive re-equilibration are much shorter than the time scale of compaction,

supporting the assumption of instantaneous magnetite-melt equilibrium in the percolation model.

Table 1 Parameters for the fractional crystallization and reactive melt infiltration models

Vertical profile		Fractional crystallization		Reactive melt infiltration model		
		Initial Cr in magma (ppm)	Thickness of magma sheet (m)	Cr in upwelling melt (ppm)	Initial Cr in magnetite (ppm)	Duration time (year)
Section-a		57	120	73.5	1240	70
Section-b		57	120	73.5	1240	58
Section-c		57	120	108	1240	51
Section-d	1-st	40	60	70	*	24
	2-nd	40	30			
	3-rd	7.5	145			

* The initial Cr content of magnetite in this profile follows the variation driven by the first, second, and third fractional crystallization events, and is shown as the coloured lines in Figure 1d.

Reactive melt infiltration. The footwall of the MML is proposed to have been permeated by interstitial melt that carried a slightly more primitive signature with it from lower parts of the UUMZ crystal pile, causing reverse zoning of cumulus plagioclase[21] and crystallization of more anorthitic interstitial grains[23]. This slightly more primitive interstitial melt would retain high Cr content because it had not yet equilibrated with magnetite in the footwall of the MML, further either enhanced by crystallization of Cr-free plagioclase in the footwall anorthositic mush or minimally diminished by the onset of crystallization of trace amounts of intercumulus magnetite. This Cr-rich melt would be discharged upward by the compaction of the footwall mush[28]. Hence, we presume an upward percolation of Cr-rich melt into the base of the recently formed magnetite mush, causing continuous modification of the Cr concentrations of magnetite grains.

263

264 We solved this reactive transport problem using the Brinkman equations coupled with
265 consideration of the dispersion around magnetite crystals via COMSOL Multiphysics for a
266 two-dimensional system with a horizontal magnetite layer sitting above an anorthositic layer
267 (Methods). The variation of porosity in the compacting magnetite cumulate as shown in
268 Figure 2a is simplified as two-layer model: a thin bottom zone (10 cm) with low porosity is
269 overlain by thick mush with a higher porosity (Fig. 1e). In our model, a slightly Cr-enriched
270 interstitial melt (~70-74 ppm Cr for the profiles in Figs. 1a-b, d; Table 1) is expelled from
271 underlying anorthositic mush at a compaction-driven velocity of ~1 m·year^{-1} [29,32-33]. The
272 basal magnetite from the section in Figure 1c contains a larger Cr content (~1.7 wt.%) and,
273 accordingly, the magnetite-saturated melt expelled from footwall mush is assumed to have
274 had a higher Cr content (~108 ppm, Table 1), which is equal to the Cr amount of the
275 intruding parental magma above the Pyroxenite Marker[43].
276

277 As a simple end-member scenario, the red lines in Figure 1a-c show the results of the
278 percolation model imposed on a pile of magnetite crystals along a one-dimensional profile
279 through the top of one of the nodes in the two-dimensional model described below (Fig. 2).
280 To identify better the influence of the percolation process, the magnetite grains in the whole
281 cumulate pile are assumed initially to be equilibrium with a Cr-depleted, evolved melt (~ 6.2
282 ppm Cr, Table 1), i.e., they initially contain a constant Cr content (~ 1240 ppm) in the whole
283 profile due to the effects of the compositional convection described above. Our percolation
284 model trends account well for the steepening of Cr compositional gradients at the bottoms of
285 all four one-dimensional sequences documented in Figure 1a-d, and the flat upper portions
286 remain as imposed by reaction with the overlying melt due to compositional convection
287 within the mush.

Lateral variations in Cr concentration. Others have inferred that concentration contours concentric around node-like structures at the base of the MML were caused by *in situ* growth that was initiated at discrete points on the floor[16,18-19]. Instead, we used our two-dimensional model of percolative reactive transport to address the alternative hypothesis that local variations in porosity in the underlying anorthosite mush may allow some sites to become preferred pathways for underlying melt during upward percolation. If Cr-rich melts flow through these nodes with a higher velocity and greater net mass flux, the grains here are able to extract more Cr than surrounding crystals, inducing lateral variations in Cr content along the base (Fig. 3a). Along with melt dispersion and upward flow in mush, this effect extends outwards to form undulations in Cr-concentration contours which gradually weaken over ~20-30 cm height (Fig. 3b-c), coinciding with the geochemical mapping on field outcrops of the MML[18]. We included an anorthosite autolith in the basal mush and considered that a solid block may impede early compaction of magnetite, leaving a high-porosity domain around the block which would enhance percolation. The resulting perturbation in the flow field led to concentric Cr enrichment around this autolith (Fig. 3d), producing spatial variations very similar to those shown by Kruger and Latypov[18-19]. This also partly accounts for the confusing phenomenon that Cr-rich growth nodes are found in the nooks beneath the autoliths but not directly on the upper surfaces of autoliths[18-19].

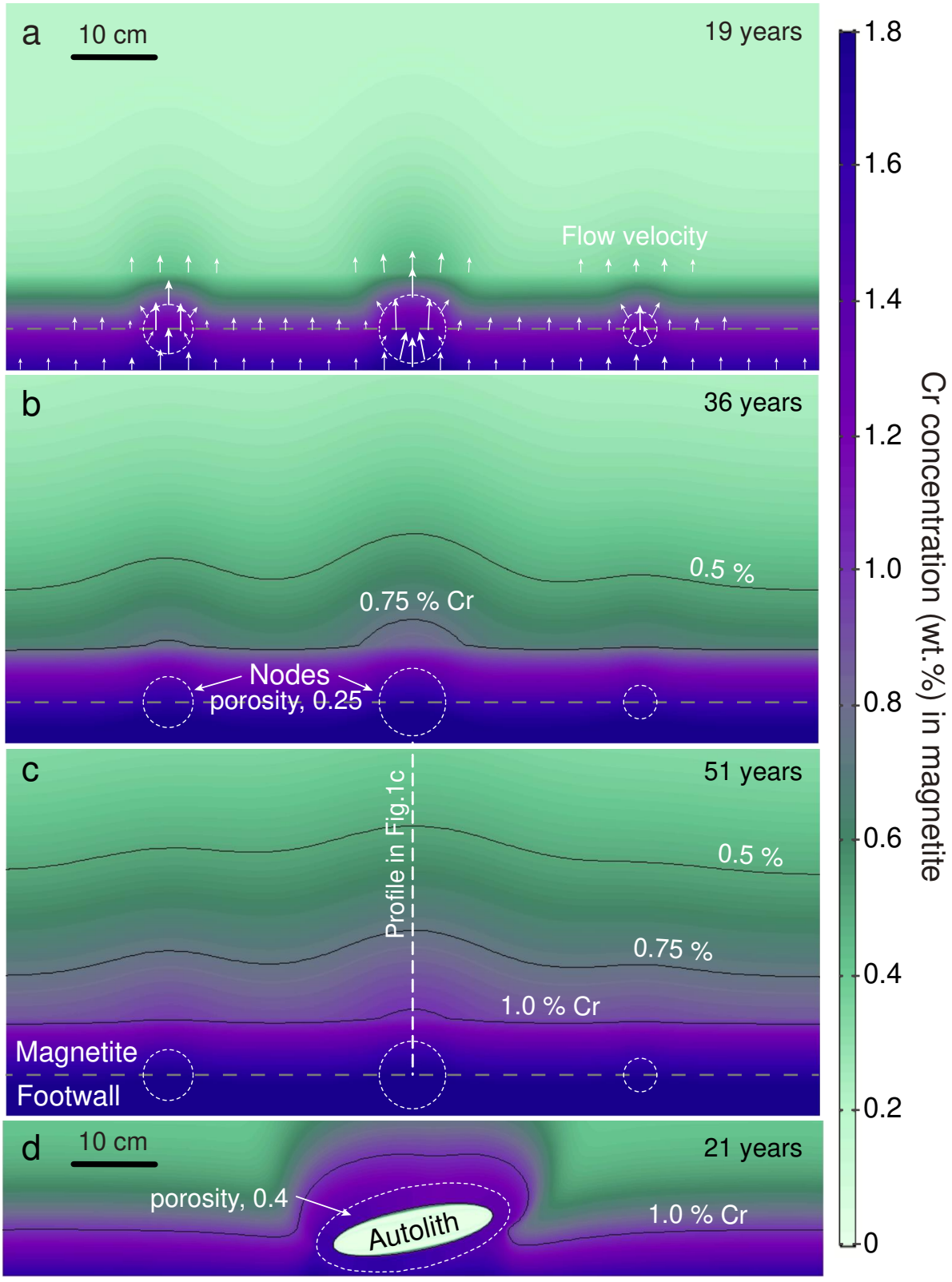

307

308 **Fig. 3** (**a**-**c**) Snapshots of modeled Cr compositional mapping for the percolation of basal

309 magnetite mush with three high-porosity spheric nodes (0.25, white dashed lines). White

310 arrows in (**a**) plot for melt flow vectors. (**d**) Cr contours drape over the anorthosite autolith

311 due its high-porosity contact zone (0.4, white dashed line) with magnetite mush. Black lines
312 represent Cr isopleths.
313
314 ***Multiple episodes of fractional crystallization combined with reactive transport.*** More
315 complex profiles than those at Magnet Heights (Fig. 1a-c) require more complex adjustments
316 to boundary conditions. We have combined the fractional crystallization model with the
317 reactive transport model to address the complexity of the Uitlugt profile, which was sampled
318 at 1 cm spacings. The large excursion in Cr content at 40 cm shown in Figure 1d, which
319 contains about 65% plagioclase, was reported not to be present in flanking boreholes by
320 McCarthy and Cawthorn (1983), who attributed it to unspecified local convective
321 fluctuations in magma composition during magnetite crystallization. To account for the
322 evident presence of three segments of the profile, each decaying from progressively lower
323 starting points, we accept the possibility that convective overturn after deposition of the first
324 ~ 40 cm of magnetite led to the start of a new episode of fractional crystallization from fresh
325 Cr-rich melt, and a third such event occurred after deposition of about 110 cm of magnetite,
326 however we do not resort to a change in magma composition every time the profile departs
327 from a perfect exponential decay. In Figure 1d we show the three initial profiles of Cr due
328 purely to fractional crystallization, as well as the trend resulting from 24 years of continued
329 evolution of Cr due to percolative reactive transport of Cr-rich intercumulus melt from below
330 (Table 1). The combined fractional crystallization and reactive transport model duplicates all
331 the observed peaks and inflections in slope of Cr variation, using only three discrete
332 crystallization sequences, for each of which the only adjustable parameter was the initial Cr
333 content of the new magma.
334
335 **Discussion and comparison with previous work**

The difference between models of *in situ* magnetite crystallization and collection of loose crystals of magnetite may seem like a moot point, but it drives at the difference between two fundamentally different mechanisms of layer formation. If crystals in layered intrusions form within the melt and are transported to their eventual resting places, the implications for petrogenesis are dramatically different than they are if crystals form *in situ* on a hard substrate. A very wide range of possibilities is consistent with deposition of a mush, but only one is permitted if crystallization proceeded *in situ*. It should be evident at this point that the match between observations and models afforded both by our models and by the previously published models places one in the uncomfortable position of having to choose between two very different sets of mechanisms to explain exactly the same observations with equal fidelity. In summary, all existing models including ours rely fundamentally on the idea that fractional crystallization of magnetite has generated the rapid and approximately exponential decay of Cr concentration in vertical profiles. The models differ in their explanations of inflections or reversals in the Cr profiles (Fig. 1) and of perturbations of Cr concentration contours due to lateral variations (Fig. 3).

Previous workers have inferred that the deposition of magnetite occurred *in situ* along the base of the magma chamber[10-12,16,18]. In these models there was no significant role for trapped liquid between magnetite crystals as they formed; lateral variations in Cr content were accounted for as resulting from initial magnetite nucleation at isolated growth centres that grew concentrically until they merged, and inflections in slope of Cr concentration in vertical profiles were accounted for by numerous adjustments to the boundary conditions[16,18]. These adjustments varied from one model to the next, but all were designed to control the supply of Cr to the fractionating magnetite. In our models, magnetite collected as discrete crystals to form an orthocumulate-textured mush during fractional crystallization; reversals of Cr

gradients in more complex profiles are accounted for by as many as three episodes of convective overturn in the overlying magma (Fig. 1d). Percolation of melt through the mush could both have erased early compositional gradients in the upper portions of thick mushes and might also have allowed upward-migrating intercumulus liquid from below to steepen the Cr concentration gradients near the base. Lateral variations in Cr concentration are accounted for by postulating that the porosity of the underlying anorthosite mush was not uniform; randomly distributed local enhancements in anorthosite permeability drove increased percolation at discrete locations in the base of the mush, generating concentrically-zoned domical patches of Cr enrichment (Fig. 3).

Geological observations can impose the primary criteria for testing these forward models. First, we consider whether it is more likely that magnetite arrived in its present location by *in situ* growth due to heterogeneous nucleation on a hard floor or by homogeneous nucleation in the melt followed by crystal settling to form a mush. The presence of plagioclase with magnetite in continuously variable proportions along with the abundance of autoliths is suggestive of co-accumulation of discrete grains due to crystal settling. The preservation of considerable relict intercumulus volume in pyroxene-poikilitic domains[13] indicates that whether it occurred heterogeneously or homogeneously, magnetite crystallization initially led to formation of an open framework through which intercumulus melt would have been free to migrate before compaction and/or adcumulus growth brought porosity down below the percolation threshold (Fig. 2b)[29,44]. In-situ crystallization experiments at low undercooling document the homogeneous nucleation of magnetite in basaltic melt even after initial heterogeneous nucleation on a solid substrate[45]. During diffusion-controlled growth, the preferred sites of incipient nucleation and rapid growth of magnetite would be expected to lie at the highest points on the surface rather than in deep reentrants under autoliths, regardless

386 of their origins as relicts of eroded floor rocks[19] or as xenoliths. Taken all together, these
387 observations and interpretations alone do not allow a firm choice between homogeneous
388 nucleation followed by crystal settling, or heterogeneous nucleation *in situ* at the magma
389 chamber floor, but we lean towards a process dominated by homogeneous nucleation from
390 the melt followed by settling of magnetite to form a highly permeable initial cumulate
391 framework.
392
393 The choices of model parameters and boundary conditions may reflect the robustness and
394 reliability of these forward models. Previous models resorted to diffusive addition of Cr from
395 convecting layers above[10-12,14-15,46]. Considering diffusive supply from a reservoir of fixed
396 size to the crystallizing magnetite Wright et al.[46] and McCarthy et al.[14] found that, to fit the
397 measured profiles for a fixed value of the Cr diffusion coefficient D in the melt, the rate of
398 crystal accumulation had to be arbitrarily constrained by the observed compositions. The rate
399 of crystal accumulation implied by the model would require as much as 3 Myr to crystallize
400 the 1 m thick MML[15]. Alternatively, Kruger and Smart[15] showed that the profile could be
401 fitted very well by assuming a continuous influx of Cr into the crystallizing layer of magma
402 from an upper layer, above a stable diffusive boundary layer, in a stratified magma
403 undergoing double diffusive convection driven by crystallization at the base and heat loss out
404 the top. However, their model could only be made to fit the observed compositional profiles
405 by adopting extremely high and unrealistic values of D_{Cr} of about 10^{-9} $m^2 \cdot s^{-1}$ whereas
406 measured values in comparable andesitic melts are about 300 times smaller (3.2×10^{-12} $m^2 \cdot s^{-1}$
407 at 1150 °C)[47]. It is possible that by changing other model parameters their curves could be
408 brought into line with measured data. The parameter least well constrained in their model is
409 the thickness of the diffusive boundary layer separating the crystallizing lower layer from the
410 layer above it. Since they never specified the value that they chose for the boundary layer

thickness it is impossible to judge whether or not it could accommodate a change sufficient to match the data using correct values for D_{Cr}. In any case, both of these previous models work only if a key model parameter such as the thickness of a hypothetical diffusive boundary layer can be adjusted at will. Evidently, without independent evidence to guide the choices of such parameters, they can be dialed in to match any profile and the modeling process becomes an arbitrary exercise in curve fitting.

Echoing the suggestion of Cawthorn[16], Kruger and Latypov[18] modeled solidification of the MML by *in situ* crystallization of magnetite directly attached to a solid substrate in a process of fractional crystallization from a well-mixed convecting reservoir of melt. As in other examples, their model would predict a continuous exponential decrease in Cr concentration and would fail to match the observed flattening of compositional profiles after the initial rapid decline (Fig. 1). To deal with this issue they added batches of fresh melt to their magma reservoir in amounts and with Cr contents arbitrarily chosen to force the model Cr trend to follow the observed trend. For example, Kruger and Latypov[18] required successive injections of four discrete magma pules with variable volumes to account for only the lowest 9 measurements in a 40-cm-thick profile (Fig. 1c). When a new pulse of magma is required in a model to account for every second data point, the model again becomes an arbitrary exercise in curve-fitting that loses predictive explanatory power. Furthermore, the two-dimensional model of magnetite crystallization had to use measured Cr concentration contours to guide their modeled crystallization sequence, rather than having the crystallization pattern governed by any physical model of diffusion-mediated crystal growth in a diffusive boundary layer.

There are weaknesses in our models as well. We have chosen boundary conditions and values for parameters like diffusivities and partition coefficients to match external constraints as

436 well as we can; however, to match the complex Cr concentration profile at Uitlugt we must
437 resort to three separate magma recharge events timed to generate the observed inflections and
438 we must perforce select a Cr content of the incoming melt to match the overall pattern. The
439 principal differences between our models and previous ones are that we minimized the
440 number of adjustable parameters (e.g., at most three magma influxes rather than one for every
441 two data points, model melt compositions fixed by equilibrium with measured mineral
442 compositions, use of experimentally measured compaction rates and diffusion coefficients)
443 and we accounted for processes widely thought to have occurred in the Upper Zone such as
444 post-cumulus melt migration and infiltration[23,28,48] which were overlooked by previous
445 approaches.
446
447 **Conclusion and implications**
448 Forward models of magmatic processes that cannot be directly observed can be valuable as
449 descriptions of what could plausibly have happened, but they cannot be regarded uncritically
450 as demonstrations of what really happened. When we are faced with multiple contradictory
451 models that can adequately generate an acceptable quantitative match to observations, we
452 must make our final choice based on the law of parsimony, also called Occam's Razor - we
453 favor the simplest hypothesis that requires the smallest number of artificially imposed
454 external constraints while simultaneously acknowledging that we cannot be sure of the
455 answer. A modeling scenario that can be set up to match the observations by setting nothing
456 more than a plausible set of initial conditions and acceptable parameter choices is greatly
457 preferable to another that requires continuous and arbitrary fine-tuning of model parameters
458 to achieve a match to observations, even more so when the arbitrary models can only succeed
459 through the adoption of physical parameters that are far outside of the ranges dictated by
460 experimental observations.

In the balance, although both sets of models can be shown to work to explain the data, we prefer our model of melt migration and reaction with a magnetite crystal mush that was itself generated in some localities by multiple pulses of deposition from a magma sheet undergoing episodic replenishments due to convective overturn. The significance of the conclusion is that it speaks to a fundamental bifurcation in our understanding of the genesis of layered intrusions - do crystals form *in situ* on solid substrates or are they formed on one place and deposited in another by transport and settling? These two concepts have dramatically important effects in controlling how we understand the formation of layered intrusions in general and, more specifically, the genesis of critically important mineral deposits of Fe, Ti, V, Ni, Cu, Co, Pt, Pd etc. The importance of *in situ* crystal growth is not unequivocally established by observations of the MML. Evidently our current knowledge of the Main Magnetite Layer does not, as yet, carry the information we need to make a definitive choice, and it is important for us to remember that as we continue to search for more definitive answers to a perplexing problem at the heart of igneous petrology.

Method

Equations for fractional crystallization model. In each increment of the fractional crystallization, the conservation of Cr mass in a closed system requires that:

$$C_{i-1}^{melt} \cdot H_{i-1} \cdot \rho_{i-1}^{melt} = C_i^{melt} \cdot k_D^{mt} \cdot (H_{i-1} - H_i) \cdot \rho_{mt} + C_i^{mt} \cdot H_i \cdot \rho_i^{melt} \quad (1)$$

where C_i^{melt}, H_i and ρ_i^{melt} are the Cr content, thickness and density of melt at *i*-th increment, respectively, and the k_D^{mt} is the partition coefficient of Cr between magnetite and melt, and here is assumed as 200 based on recent experimental measurements[24]. The density of magnetite (ρ_{mt}) is estimated as ~ 4955 kg·m^{-3} [49]. The melt density keeps decreasing due to the crystallization of denser magnetite phase, and if we make the simplifying assumption that

the partial molar volume of the Fe_3O_4 component in the melt is the same as that of magnetite, its value at the *i*-th increment can be calculated as:

$$\rho_i^{melt} = \frac{\rho_0 \cdot H_0 - \rho_{mt} \cdot (H_0 - H_i)}{H_i} \quad (2)$$

where ρ_0 is the density of initial melt (~2683 kg·m^{-3}), and H_0 is the initial thickness of melt. The thickness of the magnetite layer at the *i*-th increment is expressed as (H_0-H_i), and the Cr concentration of crystallized magnetite within this increment (C_i^{mt}) is calculated as:

$$C_i^{mt} = C_i^{melt} \cdot k_D^{mt} \quad (3)$$

Compaction time calculation. The compaction time (*t*) is the required time to reduce porosity from the initial porosity (~0.52) to a given lower value in the basal layer of a magnetite cumulate, and can be calculated as[31]:

$$t = \frac{5.471 \times 10^{18}}{10^{(14.35 \cdot \varphi)}} \times \frac{d}{h \cdot \Delta\rho} \quad (4)$$

where is φ the porosity of cumulate pile, *d* is the diameter of magnetite grains (m), *h* is the depth in crystal mush (m), and $\Delta\rho$ is the density difference between the magnetite and interstitial melt (kg·m^{-3}). On the basis of our fractional crystallization model[3], the density of the evolved melt that corresponds to the position of the MML in the Upper Zone can be estimated as ~ 2683 kg·m^{-3} via the parameterized equation from Lesher & Spera[50].

Compositional convection model. Based on the critical value of the Rayleigh number (R_a, ~25)[30,35], the minimum thickness (h_{min}) of the magnetite cumulate pile allowing compositional convection to be operative can be estimated as[29]:

$$h_{min} = \frac{R_a \cdot \mu_m \cdot D}{k \cdot g \cdot \Delta\rho'} \quad (5)$$

where μ_m is the melt viscosity (~160 Pa·s)[3,51], *D* is the effective chemical diffusivity in the melt, *k* is the permeability of crystal mush, *g* is the gravitational acceleration, and $\Delta\rho'$ is the density difference between the interstitial melt and overlaying magma. The diffusion

coefficient of Cr in melt is estimated as 3.2×10^{-12} $m^2\cdot s^{-1}$ [47], and adopted as the D here. The decrease of melt density driven by the crystallization of 2.5 wt.% magnetite from the pore melt is calculated as 58.2 $kg\cdot m^{-3}$, which can be considered as the $\Delta\rho'$. At a high porosity, the permeability of crystal mush is simplified as[33,52-53]:

$$k = d^2 \cdot \varphi^3/300 \qquad (6)$$

where d is the diameter of magnetite grains and φ is the porosity of crystal mush.

Equation for the diffusion model. For the bulk diffusion of Cr in a spherical magnetite grain with uniform initial composition and a boundary set to a different fixed composition by reaction with an infinite surrounding medium, the equilibrium degree of Cr can be expressed as the ratio of M_t (total amount of diffusing Cr entering or leaving the magnetite at time t) to M_∞ (corresponds the amount of diffusing Cr after infinite time to reach equilibrium)[38]:

$$\frac{M_t}{M_\infty} = 1 - \frac{6}{\pi^2}\sum_{n=1}^{\infty}\frac{1}{n^2}\cdot e^{-D_{Cr-mt}\cdot n^2\cdot\pi^2 t/r^2} \qquad (7)$$

where r is the radius of magnetite grain, t is the time and $D_{Cr\text{-}mt}$ is the diffusion coefficient of Cr in magnetite (~2×10^{-15} $m^2\cdot s^{-1}$)[24,37]. On the other hand, during the convective diffusion, a compositional gradient of Cr persists within a thin diffusive boundary layer around the magnetite grain, and the mass transfer (dM_{Cr}) of an element Cr via this compositional boundary layer within a short time interval (dt) can be approximated as[40]:

$$\frac{dM_{Cr}}{dt} = 4\pi r^2 \rho_m \cdot D_{Cr-melt} \cdot \frac{C_m - C_0}{\delta_{Cr}} \qquad (8)$$

where r is the magnetite radius, ρ_m is the density of melt (~ 2683 $kg\cdot m^{-3}$), $D_{Cr\text{-}melt}$ is the diffusion coefficient of Cr in melt (~ 3.2×10^{-12} $m^2\cdot s^{-1}$)[47], C_m is the Cr content of interstitial melt, C_0 is the initial Cr concentration of magnetite, and δ_{Cr} is the boundary layer thickness for Cr. The Cr flux predicted by this equation is summed for successive time intervals to

track the compositional variations of magnetite during this convective diffusion. The δ_{Cr} is mostly controlled by the strength of convection, and can be expressed as[54]:

$$\delta_{Cr} = 2r \Big/ \left[1 + (1 + \frac{2rV}{D_{Cr-melt}})^{1/3}\right] \qquad (9)$$

where V is the flow rate of interstitial melt (~ 1 m·year $^{-1}$) [29,32-33].

Reactive melt infiltration model. The Brinkman equations extend Darcy's law to model the dissipation of kinetic energy by viscous shear, which is similar to the Navier-Stokes equations, and are also connected to a set of reaction-diffusion-convection equations. Here, the Brinkman equations for steady state flow are:

$$\left\{-\nabla \cdot \frac{\mu}{\varphi}[\nabla \boldsymbol{u} + (\nabla \boldsymbol{u})^T]\right\} - \left(\frac{\mu}{k} \cdot \boldsymbol{u} + \nabla p - \boldsymbol{F}\right) = 0 \quad and \quad \nabla \cdot \boldsymbol{u} = 0 \qquad (10)$$

where μ is melt viscosity, $\boldsymbol{u}$ represents the velocity vector, p is pressure, φ is the porosity and k denotes the permeability of crystal mush. Gravity is also included in this model, and its influence is accounted for by the force term, $\boldsymbol{F}$. The grain size of magnetite is assumed as 2 mm in the model[13], and the relation between porosity and permeability follows the Kozeny-Carman model[55]. The transport of solute Cr in the migrating melt due to liquid dispersion, advection and molecular diffusion is modeled via the advection-dispersion equation:

$$\varphi \frac{\partial \gamma}{\partial t} + \nabla \cdot (-\varphi \cdot D_L \cdot \nabla \gamma + \boldsymbol{u}\gamma) = S_C \qquad (11)$$

where φ is the porosity, γ is the mass concentration of Cr in melt (kg·m^{-3}), $\boldsymbol{u}$ is the flow velocity (m·s^{-1}), D_L is the hydrodynamic dispersion tensor (m^2·s^{-1}), and S_C represents the quantity of Cr added per unit volume of porous medium per unit time at the bottom of magnetite cumulate pile (kg·m^{-3}·s^{-1}). The hydrodynamic dispersion tensor (D_L) describes the combined influences of the chemical diffusivity in the melt and the mechanical dispersivity via grain-scale flow in porous media. Hence, the diagonal components of the D_L are controlled by the diffusion coefficient of Cr in the andesitic melt (~ 3.2×10^{-12} m^2·s^{-1})[47], and

554 the dispersivities along the longitudinal and transverse flows. Previous work demonstrated a
555 systematic increase of the longitudinal dispersivity with the corresponding observational
556 scale of porous media[56], and we assume ~0.1 and ~0.4-0.6 m for the two layers in modeled
557 mush, respectively (Fig. 1e). The transverse dispersivity in experiments is typically an order
558 of magnitude smaller than that of longitudinal dispersivity[57], which is also adopted here.
559
560 **Data availability:**
561 All data shown here was obtained from the cited references.
562
563 **References:**

564 1. Namur, O. et al. Igneous layering in basaltic magma chambers. In: Chalier, B., Namur, O.,
565 Latypov, R., and Tegner, C. (eds) Layered Intrusions, 1st edn. Springer, pp. 75-152
566 (2015).
567 2. Mungall, J. E., Kamo, S. L. & McQuade, S. U-Pb geochronology documents out-of-
568 sequence emplacement of ultramafic layers in the Bushveld Igneous Complex of
569 South Africa. *Nat. Commun.* ***7***, 13385 (2016).
570 3. Yao, Z. S., Mungall, J. E. & Jenkins, M. C. The Rustenburg Layered Suite formed as a
571 stack of mush with transient magma chambers. *Nat. Commun.* ***12***, 505 (2021).
572 4. Latypov, R., Chistyakova, S. & Mukherjee, R. A novel hypothesis for origin of massive
573 chromitites in the Bushveld Igneous Complex. *J. Petrol.* ***58***, 1899-1940 (2017).
574 5. Latypov, R., Chistyakova, S., Namur, O. & Barnes, S. Dynamics of evolving magma
575 chambers: textural and chemical evolution of cumulates at the arrival of new liquidus
576 phases. *Earth-Sci. Rev.* ***210***, 103388 (2020).
577 6. Boudreau, A. E. & McCallum, I. S. Concentration of platinum-group elements by
578 magmatic fluids in layered intrusions. *Econ. Geol.* ***87***, 1830-1848 (1992).
579 7. Mungall, J. E. Kinetic controls on the partitioning of trace elements between silicate and
580 sulfide liquids. J. Petrol. 43, 749-768 (2002).
581 8. Mungall, J. E. & Naldrett, A. J. Ore deposits of the platinum-group elements. *Elements* ***4***,
582 253-258 (2008).
583 9. Wager, L. R. & Brown, G. M. Layered igneous rocks. Oliver & Boyd, Edinburgh London,

584 p. 588 (1968).
585 10. Cawthorn, R. G. & McCarthy, T. S. Variations in Cr content of magnetite from the Upper
586 Zone of the Bushveld Complex – Evidence for heterogeneity and convection currents
587 in magma chambers. *Earth Planet. Sci. Lett.* **46**, 335-343 (1980).
588 11. Cawthorn, R. G. & McCarthy, T. S. Bottom crystallization and diffusion control in
589 layered complexes: Evidence from Cr distribution in magnetite from the Bushveld
590 Complex. *Trans. Geol. Soc. S. Afr.* ***84***, 41-50 (1981).
591 12. McCarthy, T. S. & Cawthorn, R. G. The geochemistry of vanadiferous magnetite in the
592 Bushveld Complex: Implications for crystallization mechanisms in layered complexes.
593 *Miner. Depos.* ***18***, 505-518 (1983).
594 13. Reynolds, I. M. The nature and origin of titaniferous magnetite-rich layers in the Upper
595 Zone of the Bushveld Complex: A review and synthesis. *Econ. Geol.* ***80***, 1089-1108
596 (1985).
597 14. McCarthy, T. S., Cawthorn, R. G., Wright, C. J. & Mclver, J. R. Mineral layering in the
598 Bushveld Complex: Implications of Cr abundances in magnetite from closely spaced
599 magnetitite and intervening silicate-rich layers. *Econ. Geol.* ***80***, 1062-1074 (1985).
600 15. Kruger, F. J. & Smart, R. Diffusion of trace elements during bottom crystallization of
601 double-diffusive convection systems: the magnetitite layers of the Bushveld Complex.
602 *J. Volcanol. Geotherm. Res.* ***34***, 133-142 (1987).
603 16. Cawthorn, R. G. Growth nodes at the base of magnetitite layers in the Upper Zone of the
604 Bushveld Complex. *S. Afr. J. Geol.* ***97***, 455-461 (1994).
605 17. Tegner, C., Cawthorn, R.G. & Kruger, F. J. Cyclicity in the Main and Upper Zone of the
606 Bushveld Complex, South Africa: crystallization from a zoned magma sheet. *J. Petrol.*
607 ***47***, 2257-2279 (2006).
608 18. Kruger, W. & Latypov, R. Fossilized solidification fronts in the Bushveld Complex argue
609 for liquid-dominated magmatic systems. *Nat. Commun.* ***11***, 2909 (2020).
610 19. Kruger, W. & Latypov, R. Magmatic karst reveals dynamics of crystallization and
611 differentiation in basaltic magma chambers. *Sci. Rep.* ***11***, 7341 (2021).
612 20. Vantongeren, J. A., Mathez, E. A. & Kelemen, P. B. A felsic end to Bushveld
613 differentiation. *J. Petrol.* ***51***, 1891-1912 (2010).
614 21. Harney, D., Von Gruenewaldt, G. & Merkle, R. The use of plagioclase composition as an
615 indicator of magmatic processes in the Upper Zone of the Bushveld Complex.
616 Mineral. Petrol. 56, 91-103 (1996).
617 22. Maila, R. P. Geochemistry of magnetitite layers in the Upper Zone of the Bushveld

618 Complex, South Africa. Thesis, Univ. Witwatersrand (2015).
619 23. Vukmanovic, Z., Holness, M. B., Stock, M.J. & Roberts, R. J. The creation and evolution
620 of crystal mush in the Upper Zone of the Rustenburg Layered Suite, Bushveld
621 Complex, South Africa, J. Petrol. 60, 1523-1542 (2019).
622 24. Sievwright, R. H., O'Neill, H. S. C., Tolley, J., Wilkinson, J. J. & Berry, A. J., 2020,
623 Diffusion and partition coefficients of minor and trace elements in magnetite as a
624 function of oxygen fugacity at 1150 °C. *Contrib. Mineral. Petrol.* ***175***, 40 (2020).
625 25. Cawthorn, R. G. Cr and Sr: Keys to parental magmas and processes in the Bushveld
626 Complex, South Africa. *Lithos* ***95***, 381-398 (2007).
627 26. Balan, E. et al. The oxidation state of vanadium in titanomagnetite from layered basic
628 intrusions. *Am. Mineral.* ***91***, 953-956 (2006).
629 27. Fischer, L.A. The upper zone of the Bushveld Complex, South Africa: parental magma
630 and crystallization processes. Thesis, Gottfried Wilhelm Leibniz University (2018).
631 28. Hayes, B., Ashwal, L. D., Webb, S. J. & Bybee, G. M. Large-scale magmatic layering in
632 the Main Zone of the Bushveld Complex and episodic downward magma infiltration.
633 *Contrib. Mineral. Petrol.* ***172***, 13 (2017).
634 29. Sparks, R. S. J., Huppert, H. E., Kerr, R. C., McKenzie, D. P. & Tait, S. R. Postcumulus
635 processes in layered intrusions. *Geol. Mag.* ***122***, 555-568 (1985).
636 30. Tait, S. & Jaupart, C. Compositional convection in a reactive crystalline mush and melt
637 differentiation. *J. Geophys. Res.* ***97***, 6735-6756 (1992).
638 31. Manoochehri, S. & Schmidt, M. W. Settling and compaction of chromite cumulates
639 employing a centrifuging piston cylinder and application to layered mafic intrusions,
640 *Contrib. Mineral. Petrol.* ***168***, 1091 (2014).
641 32. Tegner, C., Thy, P., Holness, M. B., Jakobsen, J. K. & Lesher, C. E. Differentiation and
642 compaction in the Skaergaard Intrusion. *J. Petrol.* ***50***, 813-840 (2009).
643 33. Yao, Z. S., Qin, K. Z., Wang, Q. & Xue, S. Weak B-type olivine fabric induced by fast
644 compaction of crystal mush in a crustal magma reservoir. *J. Geophys. Res. Solid Earth*
645 ***124***, 3530-3556 (2019).
646 34. Sparks, R. S. J. & Huppert, H. E. Density changes during the fractional crystallization of
647 basaltic magmas: fluid dynamic implications. *Contrib. Mineral. Petrol.* ***85***, 300-309
648 (1984).
649 35. Nield, D. A. Onset of thermohaline convection in a porous medium. *Water Resour. Res.* ***4***,
650 553-560.
651 36. Butcher, A. R. & Werkle, R. K. W. Postcumulus modification of magnetite grains in the

upper zone of the Bushveld Complex, South Africa. *Lithos* ***20***, 247-260 (1987).
37. Finnigan, C. S., Breanan, J. M., Mungall, J. E. & McDonough, W. F. Experiments and models bearing on the role of chromite as a collector of Platinum Group Minerals by local reduction. *J. Petrol.* ***49***, 1647-1665 (2008).
38. Crank, J. The mathematics of diffusion. Oxford University press, p. 414 (1979).
39. Costa, F., Dohmen, R. & Chakraborty, S. Time scales of magmatic processes from modeling the zoning patterns of crystals. *Rev. Mineral. Geochem.* ***69***, 545-594 (2008).
40. Zhang, Y. X. Toward a quantitative model for the formation of gravitational magmatic sulfide deposits. *Chem. Geol.* ***391***, 56-73 (2015).
41. Cawthorn, R. G., McCarthy, T. S. & Davies, G. Vertical chemical gradients in a single grain of magnetite from the Bushveld Complex, South Africa. *Mineral. Mag.* ***47***, 27-34 (1983).
42. Grove, T. L., Baker, M. B. & Kinzler, R. J. Coupled CaAl-NaSi diffusion in plagioclase feldspar: Experiments and applications to cooling rate speedometry. *Geochim. Cosmochim. Acta* ***48***, 2113-2121 (1984).
43. Nex, P. A. M., Cawthorn, R. G. & Kinnaird, J. A. Geochemical effects of magma addition: compositional reversals and decoupling of trends in the Main Zone of the western Bushveld Complex. *Mineral. Mag.* ***66***, 833-856 (2002).
44. Cheadle, M. J., Elliott, M. T. & McKenzie, D. Percolation threshold and permeability of crystallizing igneous rocks: The importance of textural equilibrium. *Geology* ***32***, 757-760.
45. Polacci, M. et al. Crystallisation in basaltic magmas revealed via in situ 4D synchrotron X-ray microtomography. *Sci. Rep.* ***8***, 8377 (2018).
46. Wright, C. J., McCarthy, T. S. & Cawthorn, R. G. Numerical modelling of trace element fractionation during diffusion controlled crystallization. *Comput. Geosci.* ***9***, 367-389 (1983).
47. Koepke, J. & Behrens, H. Trace element diffusion in andesitic melts: an application of synchrotron X-ray fluorescence analysis. *Geochim. Cosmochim. Acta* ***65***, 1481-1498 (2021).
48. Maier, W. D., Barnes, S. J., Muir, D., Savard, D., Lahaye, Y. & Smith, W. D. Formation of Bushveld anorthosite by reactive porous flow. *Contrib. Mineral. Petrol.* ***176***, 3 (2021).
49. Niu, Y. L. & Batiza, R. In situ densities of MORB melts and residual mantle: Implications for buoyancy forces beneath Mid-Ocean Ridge. *J. Geol.* ***99***, 767-775.
50. Lesher, C. E. & Spera, F. J. Thermodynamic and transport properties of silicate melts and

magma. In: Sigurdsson, H. et al. (eds) *The Encyclopedia of Volcanoes*, 2nd. London Academic Press, 113-142 (2015).
51. Giordano, D., Russell, J. K. & Dingwell, D. B. Viscosity of magmatic liquids: A model. *Earth Planet. Sci. Lett.* ***271***, 123-134.
52. McKenzie, 1985. The extraction of magma from the crust and mantle. *Earth Planet. Sci. Lett.* ***74***, 81-91.
53. Water, D. A. & Watson, E. B. Grain-scale permeabilities of textually equilibrated, monomineralic rocks. *Earth Planet. Sci. Lett.* ***164***, 591-605.
54. Zhang, Y. X. & Xu, Z. J. Kinetics of convection crystal dissolution and melting, with applications to methane hydrate dissolution and dissociation in seawater. *Earth Planet. Sci. Lett.* ***213***, 133-148.
55. Costa, A. 2006. Permeability-porosity relationship: A reexamination of the Kozeny-Carman equation based on a fractal pore-space geometry assumption. *Geophys. Res. Lett.* ***33***, L02318.
56. Gelhar, L. W., Welty, C. & Rehfeldt, K.R., 1992, A critical review of data on field-scale dispersion in aquifers. *Water Resour. Res.* ***28***, 1955-1974 (1992).
57. DePaolo, D. J. High-frequency isotopic variations in the Mauna Kea tholeiitic basalt sequence: Melt zone dispersivity and chromatography. *J. Geophys. Res.* ***101***, 11855-11864.

Author contributions:

J.E.M. and Z.-S.Y. discussed the concepts; Z.-S.Y. performed modeling calculations. J.E.M. and Z.-S.Y. wrote the manuscript.

Competing interests:

The authors declare no competing interests.

Materials and correspondence:

Requests should be addressed to J.E.M.